Wetting on nanorough surfaces

S. M. M. Ramos* and E. Charlaix
Département de Physique des Matériaux (UMR CNRS 5586), Université Lyon I, 69622 Villeurbanne Cedex, France

A. Benyagoub and M. Toulemonde
CIRIL, Boîte Postale 5133, F-14040 Caen Cedex 5, France

(Received 7 March 2002; revised manuscript received 3 December 2002; published 19 March 2003)

We investigate the wetting properties of random nanostructured surfaces, with particular attention devoted to the phenomenon of contact angle hysteresis. For this purpose, solid substrates were initially tailored at a nanometric scale by using swift heavy ion irradiation which produced a random distribution of defects. We characterize the wetting properties of water on these heterogeneous surfaces by an average spreading parameter and by the contact angle hysteresis. For weak values of the areal density of defects ϕ_d, the hysteresis grows linearly with ϕ_d, indicating that the defects pin the contact line individually. However, at higher values of ϕ_d, collective pinning effects appear and the hysteresis decreases with increasing ϕ_d. We show that in the linear regime our experimental results are in good quantitative agreement with theoretical predictions for contact angle hysteresis induced by a single isolated defect on a solid surface.

DOI: 10.1103/PhysRevE.67.031604 PACS number(s): 68.08.Bc, 68.37.−d

I. INTRODUCTION

When a small drop of liquid is deposited on a solid surface two different behaviors can be identified: either the liquid spreads completely, or it remains unspread and the fluid interface meets the solid surface with a finite contact angle. In this latter case, the value of the contact angle is usually not uniquely defined and depends on the history of the motion of the three-phase contact line on the solid surface. This hysteretic behavior of the contact angle is commonly attributed to anchoring of the fluid interface on defects of the solid surface, such as chemical heterogeneities or roughness [1].

The wetting of heterogeneous surfaces has been a topic of renewed interest in the last two decades. This interest has largely been motivated by similarities between the motion of a three-phase line in the presence of pinning defects on a solid surface and the more general problem of elastic dynamics in a random force field, such as vortices in supraconductors, fracture propagation, etc. [2,3]. Therefore much theoretical and experimental work has been devoted to investigation of the motion of a fluid interface on a heterogeneous surface and of the contact angle hysteresis (CAH) [3–13]. From an experimental point of view, it has been shown that chemical heterogeneities and geometrical defects (roughness) do not have a similar effect on CAH. The experimental investigations of Dettre and Johnson [4] on paraffin wax surfaces of various roughness showed that the CAH is not a monotonic function of the surface roughness. While for weakly rough surfaces the CAH increases with the amplitude of roughness, it goes through a maximum and decreases when the roughness is further increased. A similar effect was later reported by de Jonghe *et al.* and attributed to composite wetting, i.e., the formation of air bubbles at the solid-liquid interface and/or liquid patches at the solid-air interface [5]. Composite wetting has been studied experimentally by Bico *et al.* on tailored surfaces with periodic roughness at the microscopic scale [7,8]. They developed quantitative laws for the advancing contact angle in situations of composite wetting, which generalize the so-called Wenzel law for the equilibrium contact angle on a rough surface [9]. However, such a quantitative understanding of the effects of roughness and composite wetting on the hysteresis of the contact angle is still lacking.

The goal of the present work is to understand the influence of nanometric defects on the wetting properties of a solid surface. Indeed, the studies of heterogeneous wetting realized up to now deal essentially with surfaces structured at the microscopic scale, with patterns of a few tens of micrometers in size. Experimental investigations taking into account roughness effects at a nanometer scale are still limited, probably because such studies are faced with the difficulty of obtaining rough surfaces having a controlled (in size and in concentration) distribution of nanostructures. However, the investigation of wetting on nanopatterned surfaces is of interest in many fundamental and applied situations. On one hand, the miniaturization of flow systems in microfluidic devices makes an issue of monitoring the wetting properties of a surface with texture at a nanometer scale. On the other hand, the mechanism of pinning at a nanometric scale raises the problem of the effect of thermal fluctuations, as evidenced experimentally by Prevost *et al.* [13].

In the present study we have used swift heavy ion (SHI) irradiation for processing our surfaces at the nanometric scale. It is well established that the impact of these projectiles at the surface of crystalline oxides induces the formation of hillocks of a few nanometers in size [14–17]. The choice of both the solid target material and the irradiation parameters allows us to ''tailor'' the surfaces with controlled geometrical properties. More precisely, the hillock dimensions depend on both the nature of the ion and the irradiation energy, whereas the concentration of such objects is governed by the irradiated fluence. These feature make SHI a powerful tool to produce controlled nanoscale roughness. We investigate here the role played by these topographical defects in the wetting properties of solid surfaces by combining atomic

*Corresponding author. FAX: (33)472.43.15.92. Email address: ramos@dpm.univ-lyon1.fr

TABLE I. Irradiated fluence ϕ_d (hillock concentration), average distance between hillock structures D, fraction of the surface covered by the defects α, relative expansion of the irradiated surface values R^*, and contact angle (advancing and receding) data for different samples.

Sample	Fluence (ions cm^{-2})	D (nm)	α (%)	R^*	θ_A (deg)	θ_R (deg)
A	Reference surface		0	1	96	85
B	3×10^9	182	0.8	1.008	98	81
C	6×10^9	129	1.7	1.017	110	80
D	1×10^{10}	100	2.8	1.028	113	77
E	2×10^{10}	71	5.5	1.057	108	79
F	4×10^{10}	50	10.7	1.110	96	79

force microscopy AFM observations and contact angle measurements.

II. EXPERIMENT

A. Surface processing

Single crystals of $LiNbO_3$ with a low roughness value purchased from Photonetics were used. Those crystals were processed twice. First, structures of a nanometric size were created by using swift heavy ion irradiation at Grand Accélérateur National d'lons Lourds (GANIL). As shown in previous studies of the effects of SHI on crystalline oxides, the high density of energy transferred by the projectile ion to the target electrons induces atomic motion and latent track formation along the projectile trajectory. These tracks consist of an amorphous core surrounded by a strained crystal zone. The hillock structure observed at the surface results from an out-of-plane expansion of the amorphous core, because the latter has a lower density than the pristine crystal [14–16]. In the present work, the irradiations were performed at room temperature using ^{208}Pb ions of 500 MeV energy and fluences extending from 10^9 to 6×10^{10} ions cm^{-2}. In order to ensure the homogeneity of the irradiated surface, the ion beam was carefully scanned in both the vertical and horizontal directions over a zone of 24 cm^2, considerably larger than the sample area of about 4 cm^2. This procedure was repeatedly found to provide a uniform distribution of projectile impacts at the target surface. For the different fluences used in this work we determined the corresponding fractions of the surface covered by the defects (α) as well as the average distance (D) between two neighboring defects (given in Table I). The α values are determined from the following expression:

$$\alpha = 1 - \exp(-\phi_d A), \tag{1}$$

where A is the defect cross section and ϕ_d is the irradiation fluence. This relation assumes that (i) the defect creation results from the impact of only one projectile onto the virgin part of the surface; (ii) a damaged zone is not modified by the arrival on it of further projectiles.

Second, in order to obtain contact angles large enough to be accurately measured and to have a wide range of variation of the contact angle hysteresis, octadecyltrichlorosilane (OTS) molecules were grafted on the tailored surfaces. Prior to the OTS deposition, the samples were cleaned according to the following procedure: rinsing thoroughly in hot water with Micro90 detergent in an ultrasonic bath for ~30 min, and rinsing again in deionized water. In order to provide a reference surface the OTS molecules were also grafted on a virgin sample.

B. Surface characterization

The sample surfaces were examined using atomic force microscopy. These observations were performed on an Explorer Nanoscope microscope operating in both contact and tapping modes. The surfaces were probed under ambient conditions with pyramidal silicon nitride tips in the contact mode. AFM measurements in the tapping mode were performed with silicon tips having a nominal radius curvature of ~15 nm.

In order to investigate the wettability properties of the processed surfaces, contact angle measurements were performed using the sessile drop method. For such experiments the samples were introduced in a glass chamber and a deionized water drop was put on the substrate through a microsyringe. All measurements were made in a saturated atmosphere, allowing us to avoid evaporation problems. The three-phase contact line of the water drop was advanced or receded by adding or withdrawing a small volume (~1 μl) of water. The measurements were done optically with an accuracy of 3°. The angle values were obtained from at least four drops located at different points on the surface. This procedure allows one to take into account possible nonuniformity of the surface probed by the contact angle.

III. RESULTS AND DISCUSSION

A. Surface topography

Prior to characterizing the topographic modifications induced at the irradiated surfaces, we examined by AFM (in contact mode) both the pristine sample and the as-grafted monolayer on $LiNbO_3$ crystals, which constitute our reference surfaces. In Fig. 1 we present the AFM micrographs, obtained in the contact mode, and the corresponding surface profiles recorded on both bare and OTS grafted surfaces. The rms roughness values, measured on a scanned zone of 1 μm^2, are 0.1 and 0.13 nm, respectively. These observations

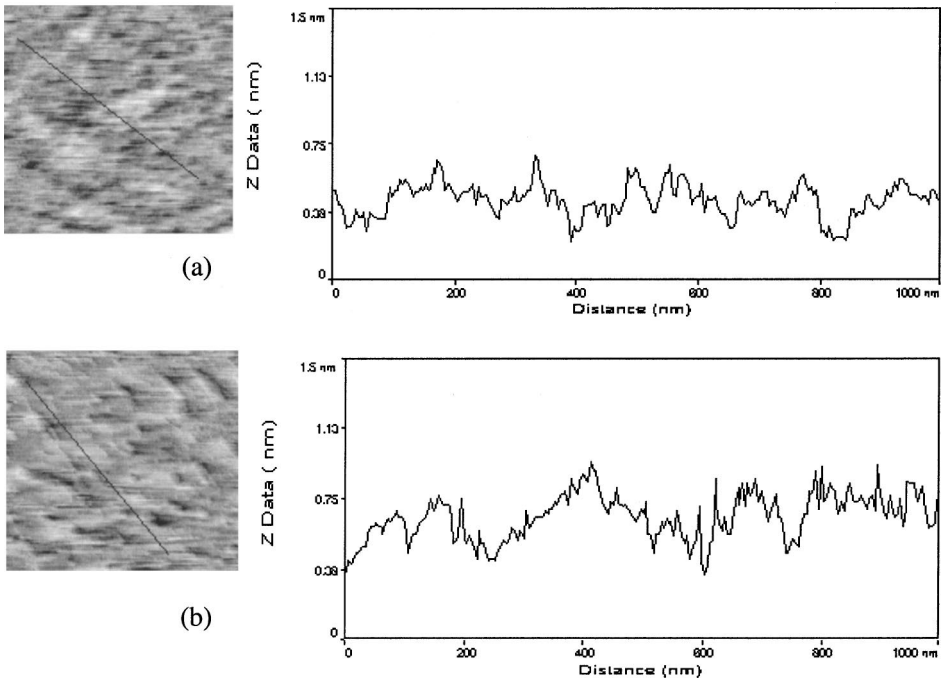

FIG. 1. Top view and surface profiles recorded on $LiNbO_3$ crystals: (a) pristine sample; (b) pristine sample after OTS grafting.

demonstrate that the OTS monolayer follows the surface topography very well, reaching about 100% total surface coverage. No significant cluster formation was observed and the surface roughness value remains low after the monolayer grafting. In order to avoid any modification induced by the probing tip, the AFM observations of the irradiated surfaces were performed only in the tapping mode. Figure 2 displays typical AFM images, in both top and perspective views, of a $LiNbO_3$ surface irradiated with Pb ions (fluence used 10^{10} Pb atoms per cm^2). A random distribution of conical-shaped hillocks with a maximal elevation of ~14 nm is clearly observed. In agreement with previous studies [14,16] using

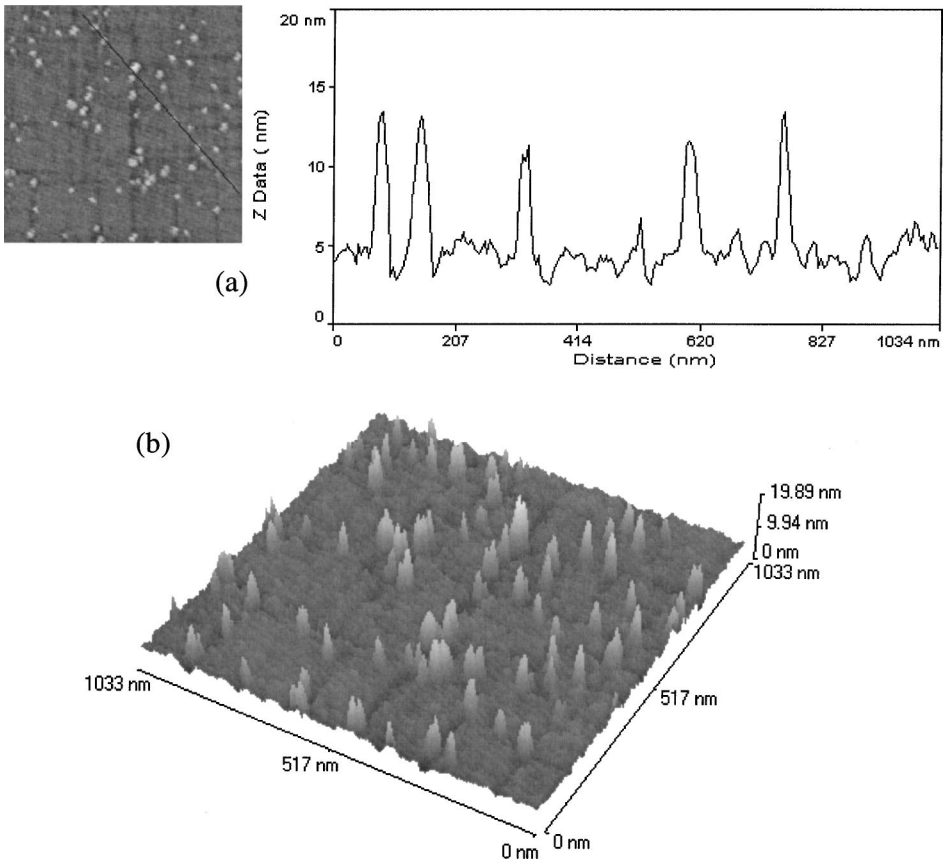

FIG. 2. (a) Top view and surface profile of as-irradiated sample ($\phi_d = 10^{10}$ Pb cm^{-2}); (b) perspective view of this sample.

both transmission electron microscopy observations, performed on a cross sectional specimen, and Rutherford backscattering spectrometry in resonant scattering conditions, these hillock structures are amorphous and present the same atomic composition as that of the pristine sample. The hillock dimensions can be extracted from an analysis of profile lines like those shown in Fig. 2. For this study, more than 80 impacts were analyzed from images obtained at four different locations. From the histograms collected from these measurements a mean basal diameter of 34 ± 4 nm and a mean height of 9.5 ± 1.5 nm were determined. It is worth noticing that as the hillocks and the probe tip apex are of similar width, the resulting image will be a convolution of the hillock and the probe tip apex. In the last few years, tip finite size effects on AFM images have been investigated in detail [18,19]. To date, different approaches are usually adopted in order to correct the raw data for the tip convolution effect. In this work we extracted the real hillock diameter from our measurements through geometric considerations based on the following hypotheses: (i) the shape of the probing tip is assumed to be parabolic with a minimum radius curvature R; (ii) the hillock structures are described as circular cones of height h and radius r. From this simple geometrical description, the observed hillock radius r_m is given by $r_m = r + Rh/2r$. An average diameter value of 19 nm was determined from our observations. Finally, the characterization of our surfaces was completed by AFM observations after OTS grafting on such tailored samples. Similarly to the abovementioned case of nonstructured samples, the film does not seem to modify the surface topography. From measurement of the hillock dimensions and the assumption of a conical shape for these asperities we calculated the relative expansion R^* (the ratio of the actual solid area to its projection) of the irradiated surfaces for all samples investigated. In this approach, we have taken $R^*=1$ for a nonirradiated surface and assumed that there is no overlap between two defects. This hypothesis is in agreement with the low defect concentration used in our investigations. For example, at the maximal fluence used (4×10^{10} cm^{-2}) the average distance between two structures is still 50 nm and the fraction of the surface covered by the defects (α) is of the order of 11%. Therefore, in these conditions the defect characteristics are independent of the fluence and the R^* values vary only with the number of defects per unity surface. The whole set of results obtained is reported in Table I.

B. Wetting properties

From the experimental measurements of both advancing (θ_A) and receding (θ_R) contact angles we have determined, for each investigated surface, two fundamental parameters for the wetting phenomenon. The first one is the average contact angle θ_0, defined as $\cos\theta_0=(\cos\theta_A+\cos\theta_R)/2$, which is related to the average spreading parameter. The second one is the contact angle hysteresis, defined as $H=\gamma(\cos\theta_R-\cos\theta_A)$. The values obtained for these two parameters in our reference (unirradiated) surface are $\theta_0=90.5°$ and $H=13.8$ mN m^{-1}, respectively. Note that in previous studies dealing with water contact angles measured on OTS monolayers grafted on a silica surface, the values of these two parameters are $\theta_0=109°$ and $H=6$ mN m^{-1} [20,21]. This difference can be ascribed to the influence of the chemical composition of the solid surface on the structure of grafted OTS layers. A quantitative study of the role played by the different parameters (such as temperature and the deposition process) on the formation of silanized monolayers on $LiNbO_3$ is now in progress.

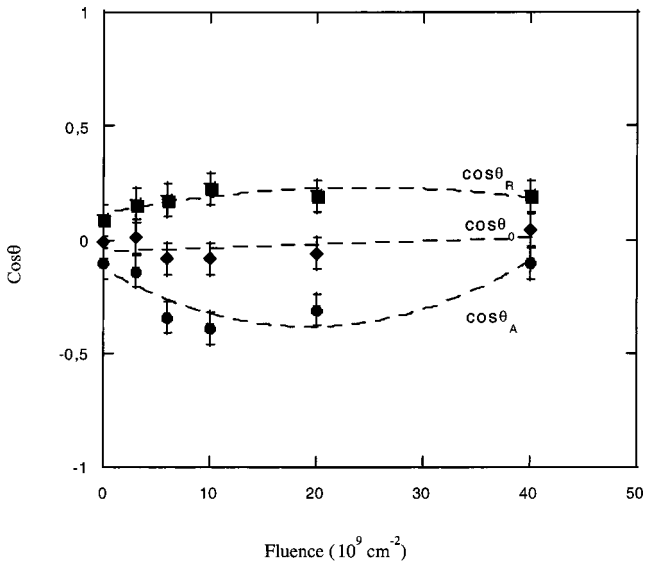

FIG. 3. Cosine of contact angle measured on the textured surface as a function of the irradiated fluence: advancing Θ_A, receding Θ, and at equilibrium Θ_0. Note that the irradiated fluences correspond to the areal concentration of the hillock structures.

1. The average contact angle

Figure 3 presents the cosine of contact angles, given in Table I, as a function of the hillock concentration. It appears that the cosine of the average contact angle varies very slightly with the defect density. This variation is not significant with respect to the resolution of the measurements. This absence of variation of the average contact angle with the number of defects shows that the wetting of the nanostructured surfaces retains a symmetrical character with respect to the advancing or receding motion of the fluid interface. This property can be explained by the fact that, since the local contact angle of the liquid on the surface θ_0 is close to 90°, advancing and receding contact lines encounter symmetric situations when moving across a purely geometrical defect of isotropic shape.

Indeed, the effect of the relative expansion of the surface R^* on the equilibrium contact angle of a liquid on a surface is usually described by Wenzel's law: $\cos\theta_{eq}=R^*\cos\theta_0$, which expresses that the real surface area is R^* times larger than the projected one. Since the R^* values of our nanotailored surfaces are close to unity, we do not expect a significant variation of this equilibrium contact angle. Bico *et al.* [7,8] studied the limit of Wenzel's law when composite wetting occurs (air bubbles or liquid drops trapped by surface defects). They showed that regimes of composite wetting

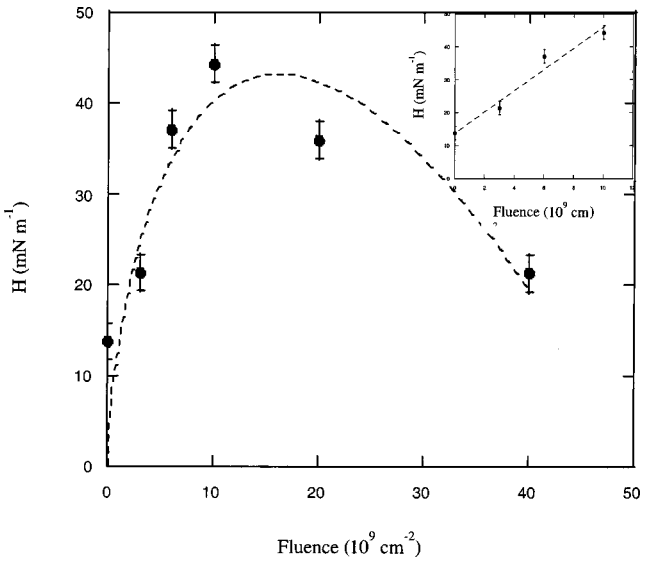

FIG. 4. Contact angle hysteresis versus the areal defect concentration (irradiated fluence).

appear at roughness values much higher than those investigated here.

Therefore the variation of the average contact angle with the defect concentration in Fig. 3 is consistent with what is expected for the wetting of a heterogeneous surface with purely geometrical defects. We cannot completely exclude, however, a chemical heterogeneity of the defects, due for instance to a small variation in the coverage of the surface by OTS molecules, which would result in a slightly different wetting property of the surface at the level of the hillocks. Assuming that in this case the average contact angle would be the same as the equilibrium contact angle, one can estimate from the data of Fig. 3 that this chemical heterogeneity should not exceed $\Delta(\gamma_{SV}-\gamma_{SI})=6$ mN/m.

2. The wetting hysteresis

The values of the contact angle hysteresis H are plotted versus the defect concentration ϕ_d in Fig. 4. Two different evolutions are identified.

For a low defect concentration $\phi_d<\phi_c$, H increases linearly with ϕ_d. This variation suggests that each defect individually pins the contact line. The slope of the straight line fitting the experimental points corresponds to the total energy W dissipated by one defect when the contact angle moves back and forth on it. From our experiments we find $W=3.2\times10^{-16}$ N m. For a detailed analysis of the hysteresis behavior in the regime of low defect concentration, we compare our experimental results with the predictions of a simplified version of the theory developed by Joanny and de Gennes [2] describing the behavior of a contact line in the presence of a single localized defect. In this approach, the equilibrium position of the triple line on a solid surface results from the action of two opposed forces: the force due to the defect, which pins the contact line, and the elastic restoring force, which tends to bring the line back to the original undisturbed position. The latter force is proportional to the amplitude of the deformation. Assuming that the topographical defect is

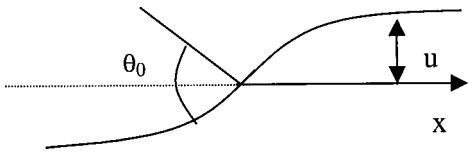

FIG. 5. A plane surface with smooth roughness.

on a planar surface, the interacting force between the defect and the triple line is provided by the following relation:

$$f=-\gamma d\sin\theta_0\sin\left(\frac{du}{dx}\right), \tag{2}$$

where d is the size of the defect while u is the defect amplitude as indicated in Fig. 5. Considering that the balance between these forces leads to hysteresis, the total energy dissipated by one defect around a hysteresis cycle is given by dimensional analysis as

$$W=\frac{f^2}{2K}, \tag{3}$$

where K, the spring constant characteristic of the restoring force, is written as $K=2\pi\gamma(1-\cos\theta_0)/\ln(L/d)$, and L is the range of deformation of the contact line.

In order to determine the value of the force on a defect, we assume that no chemical heterogeneities are created during the OTS grafting process, that is, only topographical defects are present at our surfaces. In this respect, taking into account the fact that these defects should anchor the contact line both when it advances and when it recedes, we can write the relation (3) as $f=\sqrt{KW}$. From our experimental results we determine both the spring constant K and the defect force f. For the determination of the K value, we assume that the range of deformation of the contact line L corresponds to the capillary length κ^{-1} of the liquid. By using the experimental data $\kappa^{-1}=2.7$ mm, $\gamma=72$ mN m^{-1}, and average contact angle at the reference surface $\theta_0=90.5°$, we find $K=38.4$ mN m^{-1} and $f=3.5\times10^{-9}$ N. On the other hand, we have also estimated the anchorage force f of the contact line produced by topographical defects given by relation (2). Assuming a conical shape for the hillock structures, the defect slope is $du/dx=45°$. Inserting the experimental data in relation (2) we find $f=9.7\times10^{-10}$ N. The agreement between theory and experiment is fairly good, taking into account that the theoretical expression (3) used here is only dimensional. A more quantitative analysis should take into account the actual shape of the defects. We have not performed such an analysis here, since the extraction of the exact shape of the defect from the AFM images presents difficulties due to image distortions caused by the finite size of the probing tip.

For higher defect concentration, a slope inversion is observed in the experimental curve and H decreases with increasing ϕ_d. This behavior indicates that, despite the rather large mean distance which remains between two individual impacts (e.g., for $\phi_d=2\times10^{10}$ Pb cm^{-2} the average distance between two defects is still 71 nm), an overlap in the deformation of the contact line occurs. Such hysteresis behavior is not clear to us. In this range of fluence, the defects are far from overlapping themselves significantly and their indi-

vidual characteristics remain unchanged; therefore this different regime of variation of the hysteresis has to do with the onset of collective effects in pinning. Previous studies of the collective effects in the anchoring of a contact line by several defects predict that the contact angle hysteresis should increase with the defect density, although this variation is less than linear [6,22]. On the other hand, even at the highest defect concentrations investigated here, the surface coverage by defects is still low and one cannot consider that adding new defects decreases its heterogeneity. We can think of two mechanisms that may be responsible for this regime. The first one is the ''bipolar'' character of topographical defects. The contact line motion around an isolated defect can be divided into two sequences: Initially, it takes an upward direction and the defect is seen as attractive by the contact line; subsequently, taking a downward direction, the defect is seen as repulsive and is able to anchor the contact line. These two sequences do not depend on the direction of motion of the contact line and occur in both advancing and receding motion. When a defect acts individually on the contact line its ambivalent wetting or nonwetting characteristic with respect to the flat surface has no particular consequences. But when two or more defects act collectively, the wetting side of one defect may help the contact line to untrap from the nonwetting side of another one, resulting in partial annihilation of its individual trapping efficiency. The second mechanism is the possible formation of nanobubbles at the water-OTS interface as shown in the AFM investigation by Tyrell and Attard [23]. The conditions for the formation of such nanobubbles are not yet well understood. However, since they appear at the nonwetting OTS surface one may think that their formation is favored by the presence of roughness defects in sufficiently high concentration, and that in return they screen those defects, which would result in a decrease of the contact angle hysteresis.

IV. CONCLUSION

In summary, we have shown experimentally that a random topographical distribution of nanometric defects influences the wetting properties of solid surfaces. By focusing our investigations on the phenomenon of contact angle hysteresis H we have evidenced the existence of two different regimes that depend on the defect concentration ϕ_d. The linear increase of H with ϕ_d, observed for low defect concentration, is reasonably described by a pinning-depinning process of the contact line by individual defects. The decrease of H with increasing ϕ_d, evidenced in the high-concentration regime, indicates that a destructive interaction of surface defects should occur at the contact line. These results open at least two main directions for further work. On one hand we plan to perform both numerical simulations and complementary contact angle measurements in a wider defect concentration range and with various defect sizes in order to determine quantitatively the influence of the defect interaction on the motion of the contact line on a topographically rough surface. In particular we will focus numerical work on the influence of the ''bipolar'' character of roughness defects on their collective anchoring properties. On the other hand, we intend to study the water-OTS covered $LiNO_3$ interface at the nanometric scale by noncontact mode AFM, in order to investigate the possible occurrence of composite wetting by nanobubbles and the role of small-size defects in this effect.

[1] P. G. de Gennes, Rev. Mod. Phys. **57**, 827 (1985).
[2] J. F. Joanny and P. G. de Gennes, J. Chem. Phys. **81**, 552 (1984).
[3] M. O. Robbins and J. F. Joanny, Europhys. Lett. **3**, 729 (1987).
[4] R. H. Dettre and R. E. Johnson, J. Am. Chem. Soc. **43**, 136 (1964); R. E. Johnson and R. H. Dettre, Adv. Chem. Ser. **43**, 112 (1964).
[5] V. de Jonghe, D. Chatain, I. Rivollet, and N. Eustathopoulos, J. Chim. Phys. Phys.-Chim. Biol. **87**, 1623 (1990).
[6] J.-M. di Meglio, Europhys. Lett. **17**, 607 (1992).
[7] José Bico, Christian Marzolin, and David Quéré, Europhys. Lett. **47**, 220 (1999).
[8] J. Bico, C. Tordeux, and D. Quéré, Europhys. Lett. **55**, 214 (2001).
[9] R. N. Wenzel, J. Phys. Colloid Chem. **53**, 1466 (1949).
[10] J. F. Oliver, C. Huh, and S. G. Masson, J. Colloid Interface Sci. **59**, 568 (1997).
[11] A. Paterson and M. Fermigier, Phys. Fluids **9**, 2210 (1997); A. Paterson, M. Fermigier, P. Jenffer, and L. Limat, Phys. Rev. E **51**, 1291 (1995).
[12] T. Cubaud and M. Fermigier, Europhys. Lett. **65**, 339 (2002).
[13] A. Prevost, E. Rolley, and C. Guthmann, Phys. Rev. Lett. **83**, 348 (1999).
[14] B. Canut, R. Brenier, A. Meftah, P. Moretti, S. Ould Salem, S. M. M. Ramos, P. Thevenard, and M. Toulemonde, Nucl. Instrum. Methods Phys. Res. B **91**, 312 (1994).
[15] S. M. M. Ramos, N. Bonardi, B. Canut, and S. Della-Negra, Phys. Rev. B **57**, 1 (1998).
[16] S. M. M. Ramos, N. Bonardi, B. Canut, S. Bouffard, and S. Della-Negra, Nucl. Instrum. Methods Phys. Res. B **143**, 319 (1998).
[17] C. Trautmann, J. M. Constantini, A. Meftah, K. Schwartz, J. P. Stoquert, and M. Toulemonde, in *Atomistic Mechanisms in Beam Synthesis and Irradiation of Materials*, edited by J. C. Barbour, S. Roorda, and D. Ila, Mater. Res. Soc. Symp. Proc. No. 504 (Materials Research Society, Pittsburgh, 1998), p. 123.
[18] C. Odin, J. P. Aimé, Z. El Kaakour, and T. Bouhacina, Surf. Sci. **317**, 321 (1994).
[19] D. Keller, Surf. Sci. **253**, 353 (1991).
[20] M. C. Yeh, E. J. Kramer, R. Sharma, W. Zhao, M. H. Rafailovich, J. Sokolov, and J. D. Brock, Langmuir **12**, 2747 (1996).
[21] P. Silberzan, L. Léger, D. Ausserré, and J. J. Benattar, Langmuir **7**, 1647 (1991).
[22] J. Crassous and E. Charlaix, Europhys. Lett. **28**, 415 (1994).
[23] J. W. G. Tyrell and P. Attard, Phys. Rev. Lett. **87**, 176104 (2001).